Research Square

Preprints are preliminary reports that have not undergone peer review.
They should not be considered conclusive, used to inform clinical practice,
or referenced by the media as validated information.

# Ferroptosis genes coexpressed with disulfidptosis genes form a prognostic signature in colon cancer

**Tianyang Zhi**
Changshu No.1 People's Hospital
**Yanlin Li**
Changshu No.1 People's Hospital
**Kuangyi Lu**
Changshu No.1 People's Hospital
**Qiao Chen**
Changshu No.1 People's Hospital
**Suo Wang**
Changshu No.1 People's Hospital
**Yingjie Xu**
Changshu No.1 People's Hospital
**Jiayao Zheng**
Putuo District People's Hospital, Zhoushan City, Zhejiang Province
**Jinbing Sun**
sunjbsunjb515@163.com

Changshu No.1 People's Hospital

**Research Article**

**Keywords:** Colon cancer, prognostic signature, ferroptosis, disulfidptosis, DRD4, external validation

**Posted Date:** November 18th, 2026

**DOI:** https://doi.org/10.21203/rs.3.rs-11259180/v1

**License:** This work is licensed under a Creative Commons Attribution 4.0 International License.
Read Full License

**Additional Declarations:** No competing interests reported.

# Ferroptosis genes coexpressed with disulfidptosis genes form a prognostic signature in colon cancer

Tianyang Zhi[1†], Yanlin Li[1†], Kuangyi Lu[1], Qiao Chen[1], Suo Wang[1], Yingjie Xu[1], Jiayao Zheng[2*] and Jinbing Sun[1*]

1 Department of General Surgery, Changshu No. 1 People's Hospital, Affiliated Changshu Hospital of Soochow University, 1 Shuyuan Road, Changshu, Jiangsu 215500, China

2 Putuo People's Hospital of Zhoushan City, 19 Wenkang Street, Zhejiang 316100, China

*Correspondence to Jinbing Sun (sunjbsunjb515@163.com) or Jiayao Zheng (zjy01212512@163.com)

†These authors contributed equally: Tianyang Zhi and Yanlin Li.

ORCID: Tianyang Zhi, https://orcid.org/0009-0007-9912-7472

## Abstract

Ferroptosis and disulfidptosis both depend on cystine metabolism, but the prognostic relevance of their shared transcriptional features in colon cancer remains unclear. We screened FerrDb genes for coexpression with 23 disulfidptosis-related genes in TCGA-COAD and developed a seven-gene risk score using univariable and LASSO-Cox regression. The score was externally evaluated in GSE38832. DRD4 protein expression was examined in 64 paired tumors and adjacent non-tumor tissues, and DRD4 was silenced in RKO cells. The signature comprised DRD4, FNDC5, ALOXE3, HOTAIR, GSTM1, FABP4 and MPC1. High-risk groups had shorter disease-free survival in TCGA-COAD and GSE38832 (log-rank $P < 0.0001$ and $P = 0.0056$). Areas under the curve at 1, 3 and 5 years were 0.74, 0.70 and 0.73 in TCGA-COAD and 0.74, 0.70 and 0.58 in GSE38832. DRD4 positivity was more frequent in tumors and was associated with T stage and vascular invasion. DRD4 silencing reduced cell viability, migration and invasion. The signature retained short- and intermediate-term discrimination in one external cohort, whereas its 5-year performance was limited. These findings support further multicenter evaluation of the signature and mechanistic investigation of DRD4.

**Keywords:** Colon cancer; prognostic signature; ferroptosis; disulfidptosis; DRD4; external validation

## Introduction

Reproducible biomarkers could refine risk stratification beyond pathologic stage in colon cancer. Colorectal cancer remains a leading cause of cancer incidence and mortality worldwide. [1] Colon cancer varies in driver alterations, transcriptional

subtypes, clinical course, and treatment response. [2-6] Patients with the same pathologic stage may therefore experience different outcomes. Molecular scores that retain performance across cohorts and complement clinical variables may improve individualized prognostic assessment.

Ferroptosis provides a biologically grounded source of candidate prognostic genes in colon cancer. This form of cell death is driven by iron-dependent phospholipid peroxidation. [7,8] Its regulation involves lipid remodeling, cystine uptake, the glutathione-GPX4 axis, and antioxidant systems such as FSP1. [9-15] These processes contribute to metabolic adaptation, treatment resistance, and antitumor immunity. [12,13,16,17]

Disulfidptosis and ferroptosis both depend on cystine metabolism but remain distinct forms of regulated cell death. In SLC7A11-high cells, glucose restriction can deplete NADPH and promote aberrant disulfide bonding of cytoskeletal proteins. The resulting F-actin contraction leads to cytoskeletal collapse. [18] SLC7A11-mediated cystine uptake also increases dependence on the pentose phosphate pathway and NADPH. [19] SLC7A11 may therefore suppress ferroptosis while increasing susceptibility to disulfidptosis under nutrient-limited conditions.

Several TCGA- and Gene Expression Omnibus (GEO)-based ferroptosis-related prognostic signatures have been reported for colon cancer. [20-22] Yi et al. developed a two-gene model comprising DRD4 and SLC2A3 and evaluated it in GSE17538, GSE38832, and immunohistochemical analyses. [23] However, the reproducibility and incremental value of such signatures remain uncertain.

We therefore asked whether a seven-gene risk score derived from ferroptosis genes coexpressed with disulfidptosis-related genes could stratify disease-free survival in TCGA-COAD and retain prognostic information in GSE38832. We also examined whether DRD4 protein expression differed between paired tumor and adjacent tissues and whether DRD4 silencing altered RKO cell viability, migration, and invasion.

# Results

### Identification and functional annotation of candidate coexpression genes

The prespecified thresholds ($|r| > 0.50$ and two-sided $P < 0.05$) identified 478 FerrDb ferroptosis-related genes coexpressed with at least one disulfidptosis-related gene (Fig. 1a).

Of these genes, 131 were differentially expressed between 424 colon cancers and 41 adjacent non-tumor tissues (FDR < 0.05 and absolute $\log_2$ fold change > 1). Sixty-eight genes were upregulated and 63 were downregulated (Fig. 1b).

GO cellular-component terms included basal and apical cell regions, the microvillus membrane, and basal and apical plasma membranes. Enriched molecular functions

included bile acid, iron ion, and monocarboxylic acid binding, aldo-keto reductase activity, and ferric iron binding. Leading biological processes involved responses to oxygen levels, chemical stress, inorganic substances, metal ions, oxidative stress, and iron ions (Fig. 1c).

KEGG analysis identified hypoxia-inducible factor 1 signaling, ferroptosis, interleukin-17 signaling, central carbon metabolism in cancer, unsaturated fatty acid biosynthesis, mineral absorption, and microRNAs in cancer (Fig. 1d).

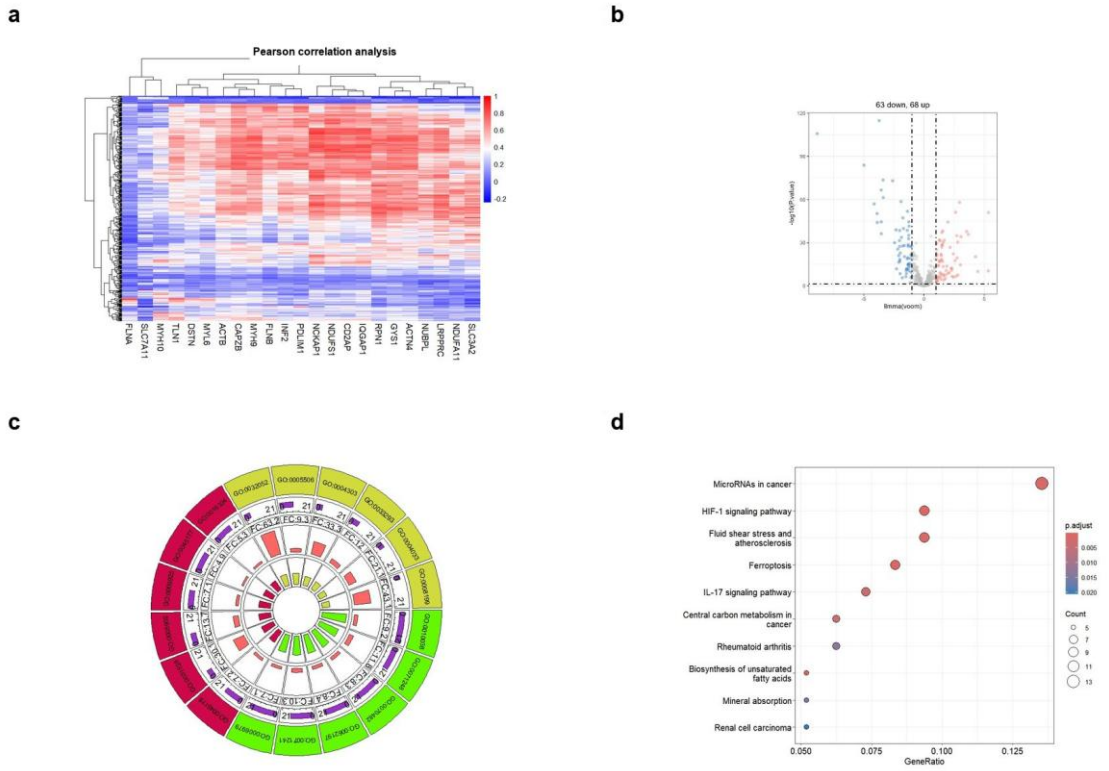



Fig. 1 Screening and functional annotation of ferroptosis genes coexpressed with disulfidptosis genes. (a) Pearson correlation heatmap of candidate genes. (b) Volcano plot of differential expression between colon cancer and adjacent non-tumor tissues (FDR < 0.05; |$\log_2$ fold change| > 1). (c) GO enrichment analysis. (d) KEGG enrichment analysis. FDR, false discovery rate; GO, Gene Ontology; KEGG, Kyoto Encyclopedia of Genes and Genomes. KEGG pathway annotations shown in panel (d) are used with permission from Kanehisa Laboratories (Ref. 262168)

**Development of the seven-gene prognostic signature**

Univariable Cox regression identified 14 genes associated with disease-free survival in TCGA-COAD (Fig. 2a). Higher expression of FABP4, TIMP1, CDKN2A, ALOXE3, HAMP, FNDC5, PANX2, DRD4, GSTM1, and HOTAIR was associated with shorter survival. Higher expression of MPC1, GDF15, SCP2, and CXCL2 was associated with longer survival.

The 14 genes were entered into LASSO-Cox regression. Ten-fold cross-validation retained DRD4, FNDC5, ALOXE3, HOTAIR, GSTM1, FABP4, and MPC1 (Fig. 2b

and c). Supplementary Table S3 presents the regression coefficients. DRD4 had the largest positive coefficient, whereas MPC1 had a negative coefficient.

The individual risk score was calculated as follows:

Risk score = (0.62874 × DRD4) + (0.55512 × FNDC5) + (0.30854 × ALOXE3) + (0.29598 × HOTAIR) + (0.10926 × GSTM1) + (0.04455 × FABP4) - (0.25369 × MPC1).

Each term denotes the standardized expression level of the corresponding gene.

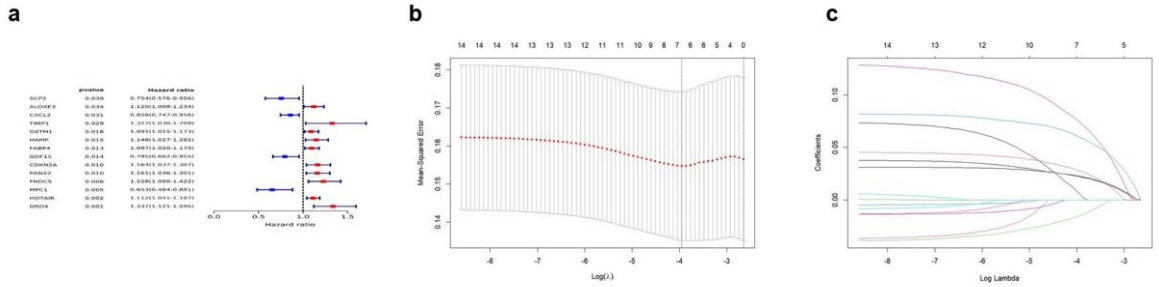



Fig. 2 Development of the seven-gene prognostic signature. (a) Forest plot of univariable Cox regression showing hazard ratios and 95% confidence intervals. (b) Ten-fold cross-validation for selection of the LASSO penalty parameter. (c) LASSO coefficient profiles. CI, confidence interval; HR, hazard ratio; LASSO, least absolute shrinkage and selection operator

**Risk stratification and external cohort evaluation**

The TCGA-COAD median risk score (-0.09) divided patients into high- and low-risk groups (Fig. 3a). Deaths were more frequent and survival times were shorter as the risk score increased (Fig. 3c). DRD4, FNDC5, ALOXE3, HOTAIR, GSTM1, and FABP4 were generally more highly expressed in the high-risk group, whereas MPC1 showed the opposite pattern (Fig. 3e).

GSE38832 showed similar distributions of risk scores, survival events, and signature-gene expression when the TCGA-COAD cutoff was applied (Fig. 3b, d, and f).

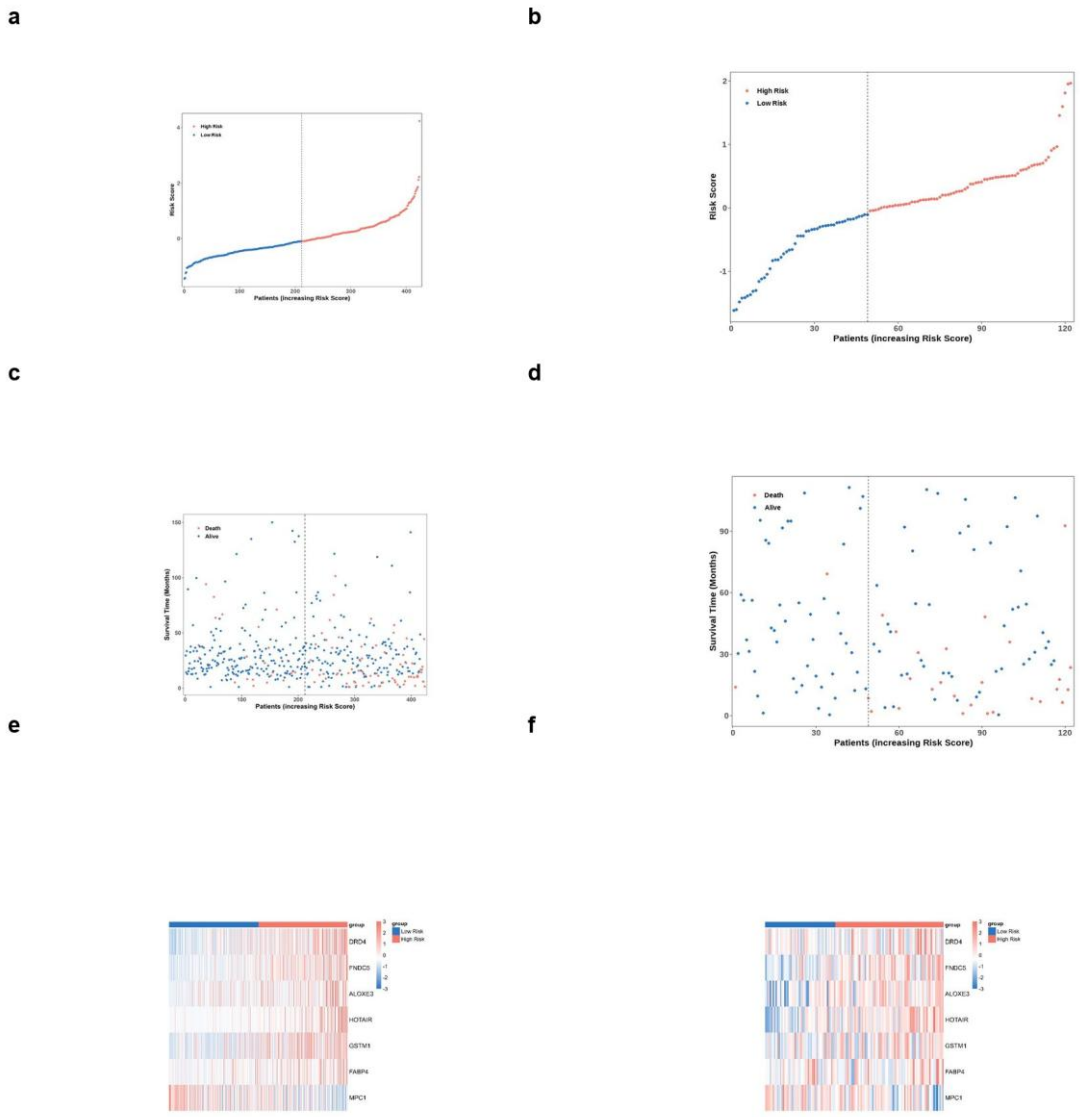



Fig. 3 Risk stratification in the TCGA training cohort and GSE38832 external evaluation cohort. (a, b) Patient distributions ordered by increasing risk score. (c, d) Survival status and follow-up time. (e, f) Heatmaps of standardized expression of the seven signature genes. Dashed lines indicate the prespecified median cutoff from the training cohort

## Prognostic performance of the seven-gene signature

Disease-free survival was shorter in the TCGA-COAD high-risk group than in the low-risk group (log-rank $P < 0.0001$; Fig. 4a). The same direction of survival separation was observed in GSE38832 (log-rank $P = 0.0056$; Fig. 4b).

In TCGA-COAD, the 1-, 3-, and 5-year time-dependent AUCs were 0.74, 0.70, and 0.73, respectively (Fig. 4c). The corresponding AUCs in GSE38832 were 0.74, 0.70, and 0.58 (Fig. 4d). The score therefore retained discrimination at 1 and 3 years in GSE38832, but 5-year discrimination was limited.

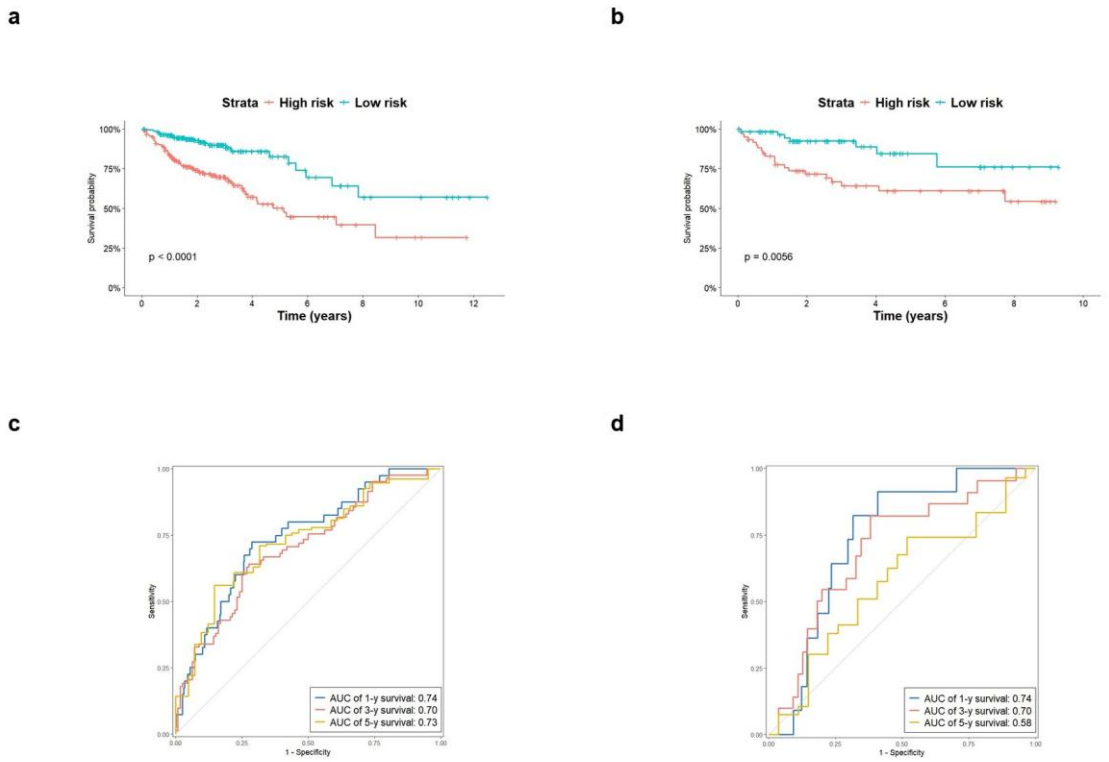



Fig. 4 Survival stratification and time-dependent discrimination of the seven-gene signature. (a, b) Kaplan-Meier disease-free survival curves in the TCGA training and GSE38832 external cohorts. (c, d) Time-dependent ROC curves at 1, 3, and 5 years in the training and external cohorts. AUC, area under the curve; ROC, receiver operating characteristic

**Independent prognostic value and combined nomogram**

Age, tumor stage, and the risk score were associated with disease-free survival in univariable Cox models, whereas sex was not (Fig. 5a). After adjustment for age and tumor stage, the risk score remained independently associated with poorer disease-free survival (HR, 2.05; 95% CI, 1.56-2.68; P < 0.001; Fig. 5b).

The nomogram combining age, tumor stage, and risk score yielded 1-, 3-, and 5-year AUCs of 0.82, 0.83, and 0.82, respectively (Fig. 5c-f). Calibration plots showed approximate agreement between predicted and observed probabilities across the displayed range (Fig. 5g).

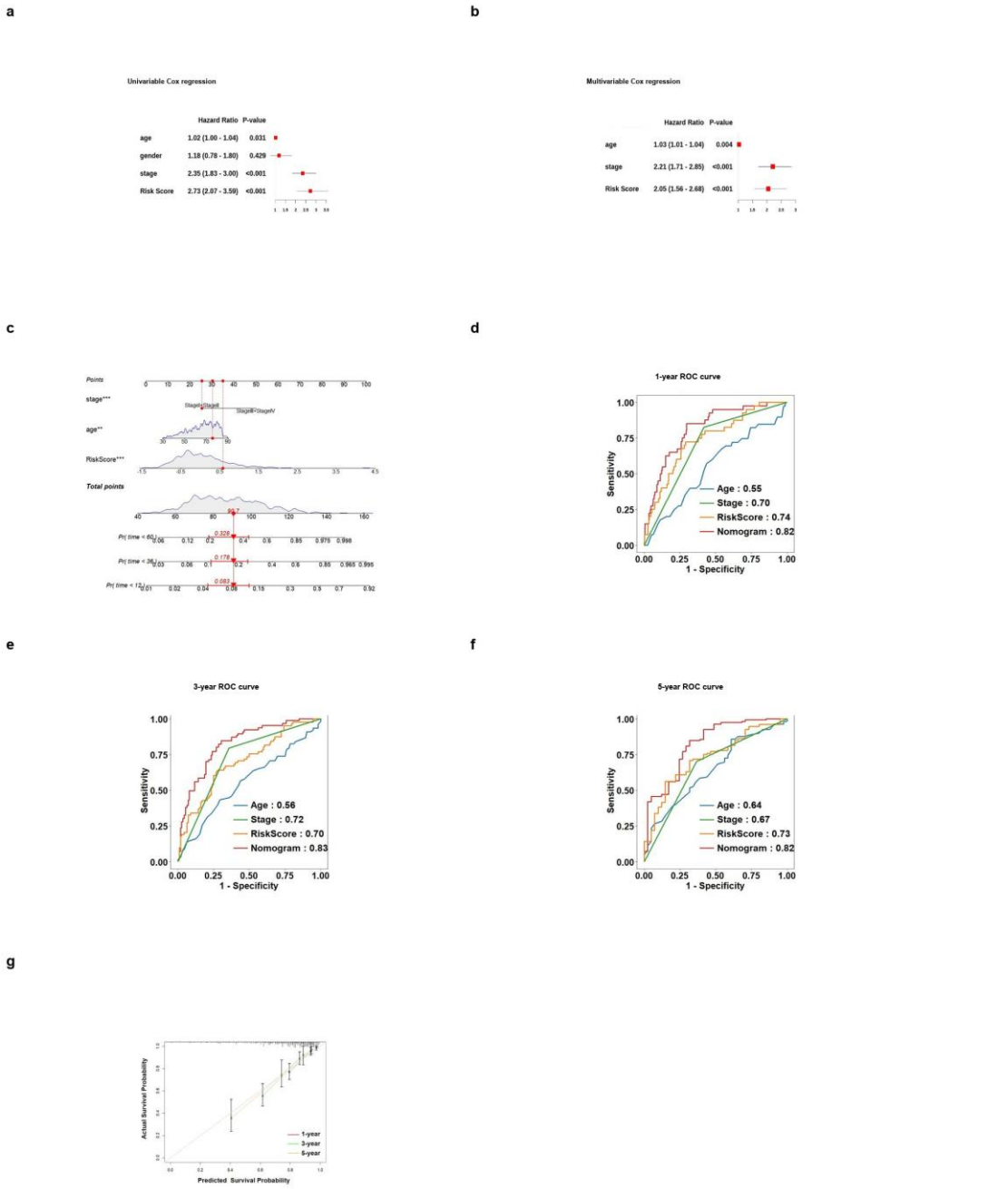



Fig. 5 Independent prognostic value of the seven-gene risk score and the combined nomogram. (a, b) Univariable and multivariable Cox regression analyses. (c) Nomogram incorporating age, tumor stage, and risk score. (d-f) ROC curves at 1, 3, and 5 years. (g) Calibration curves at 1, 3, and 5 years. CI, confidence interval; HR, hazard ratio; ROC, receiver operating characteristic

## Biological pathways associated with the risk signature

Within GO gene sets, the high-risk group was enriched for aerobic respiration, mitotic nuclear division, oxidative phosphorylation, positive regulation of the cell cycle, and mitochondrial protein complex-related pathways (Fig. 6a).

KEGG gene sets in the high-risk group were enriched for cytokine-related signaling, non-cytochrome P450-dependent drug metabolism, peroxisomal pathways, retinol metabolism, and starch and sucrose metabolism (Fig. 6b). Reactome analysis identified cell-cycle checkpoints, receptor-binding chemokines, DNA replication, prereplicative-complex activation, and the G2/M checkpoint (Fig. 6c).

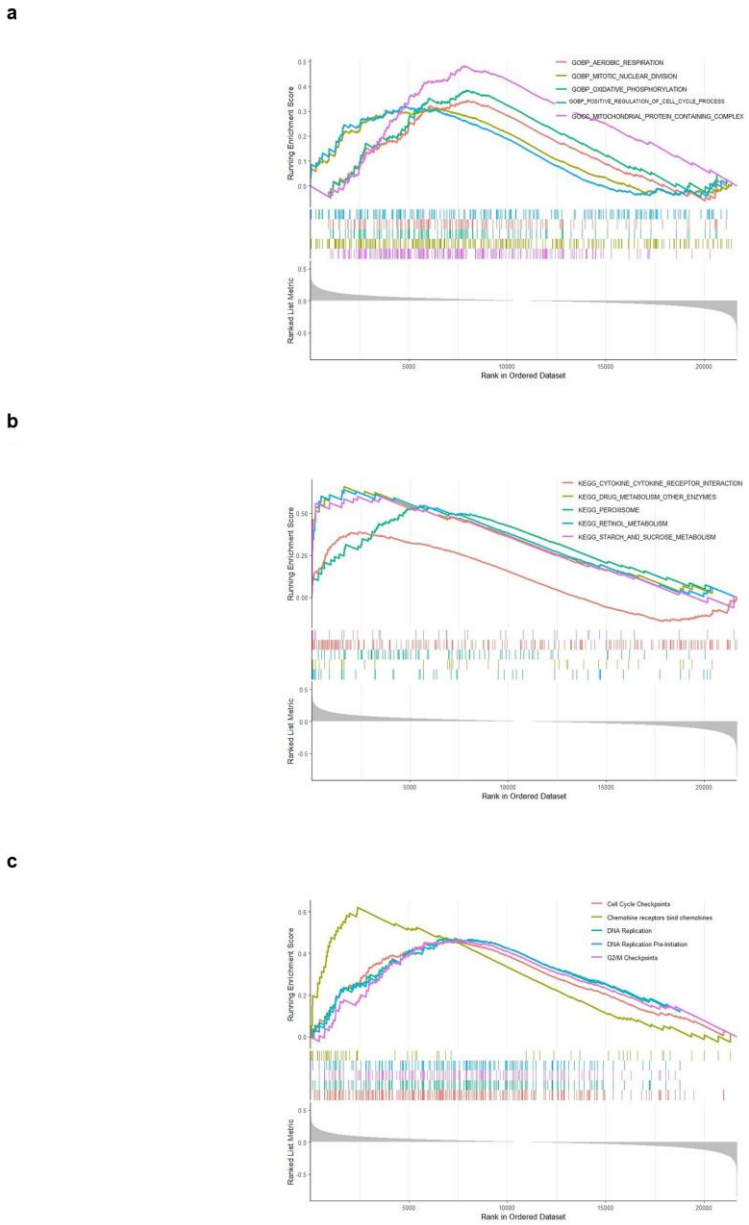



Fig. 6 GSEA results for the high-risk group relative to the low-risk group. (a) GO gene sets. (b) KEGG gene sets. (c) Reactome gene sets. Curves show representative enriched pathways. GSEA, gene set enrichment analysis. KEGG pathway annotations shown in panel (b) are used with permission from Kanehisa Laboratories (Ref. 262168)

## Expression patterns of regulated cell death-related genes

Ferroptosis-related gene expression differed between risk groups. AIFM2, GPX4, HSPB1, and HSF1 were more highly expressed in the high-risk group, whereas ACSL4, LPCAT3, and SQLE were expressed at lower levels (all $P < 0.05$; Fig. 7a). This pattern was consistent with greater transcriptional activity of defenses against lipid peroxidation.

Genes related to disulfidptosis and actin-cytoskeleton regulation also differed between risk groups. NCKAP1, RAC1, ABI1, BRK1, ACTR2, ACTR3, and CDC42 were more highly expressed in the high-risk group. NDUFA11 and GYS1 were expressed at lower levels (all $P < 0.05$; Fig. 7b). These differences may reflect distinct metabolic and cytoskeletal states.

## Immune features and computationally predicted immunotherapy response

Single-sample GSEA identified differences in several immune-cell enrichment scores between risk groups (all $P < 0.05$; Fig. 7c). These populations included activated CD4+ T cells, CD56bright and CD56dim natural killer cells, memory B cells, T helper 17 cells, central memory CD4+ T cells, natural killer T cells, natural killer cells, and neutrophils. Scores for activated CD4+ T cells, CD56bright natural killer cells, memory B cells, T helper 17 cells, and neutrophils were lower in the high-risk group.

Immune checkpoint-related genes also differed between risk groups (all $P < 0.05$; Fig. 7d). BTNL9, CD276, CD40, HLA-DPB1, HLA-DQB1, SIRPA, TNFRSF14, TNFRSF18, TNFRSF4, and TNFSF14 were more highly expressed in the high-risk group. CD47, CD80, CEACAM1, and TNFSF18 were expressed at lower levels.

TIDE scores were higher in the high-risk group than in the low-risk group ($P = 0.044$; Fig. 7e). Higher scores indicated stronger computationally inferred immune-evasion features and a lower predicted probability of response to immune checkpoint blockade.

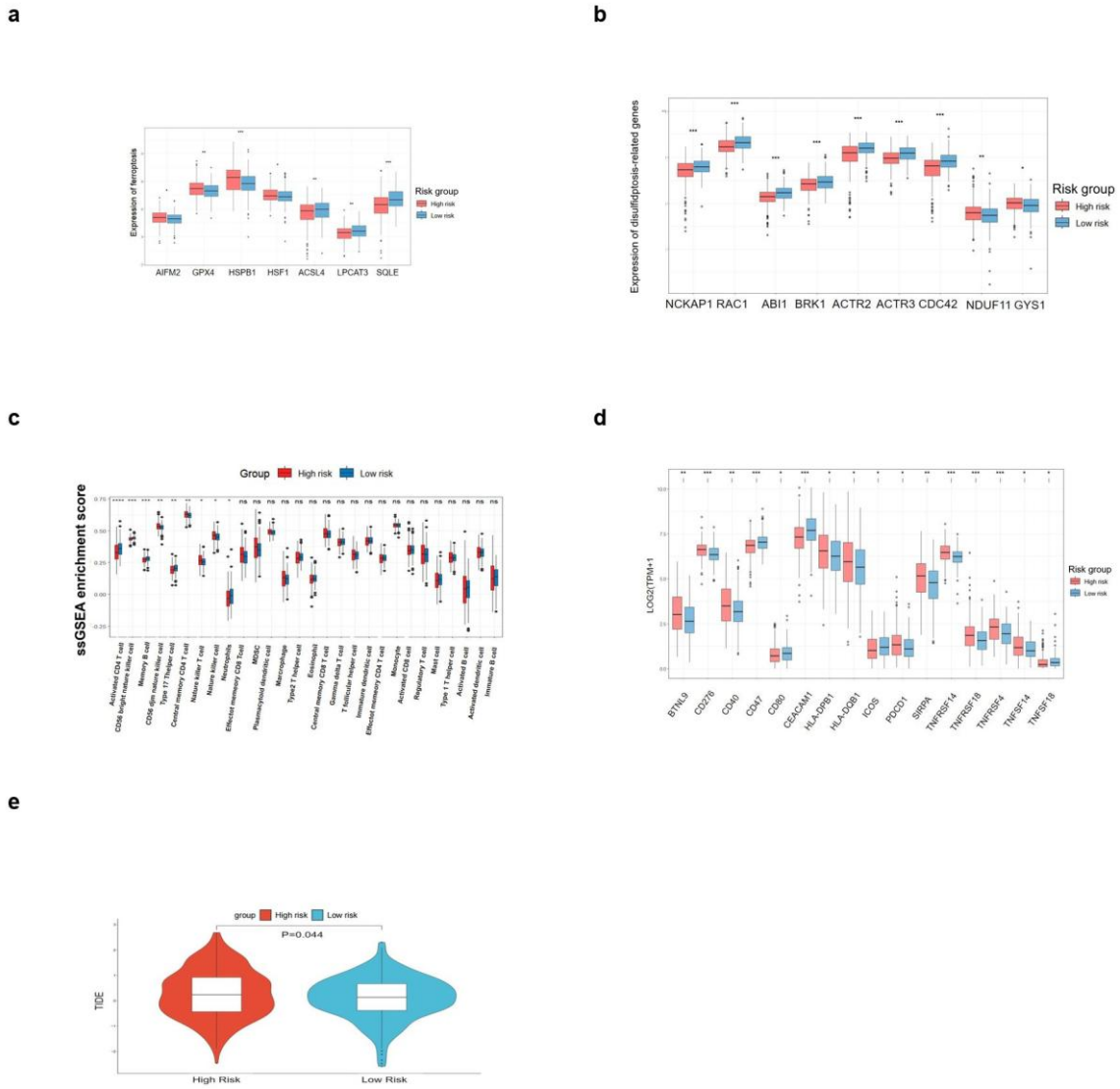



Fig. 7 Regulated cell death and immune features associated with the risk score. (a) Representative ferroptosis-related genes. (b) Disulfidptosis- and cytoskeleton-related genes. (c) ssGSEA-inferred immune-cell enrichment scores. (d) Immune checkpoint-related genes. (e) TIDE scores. Box plots show the distributions between groups. ns, not significant; *P < 0.05; **P < 0.01; ***P < 0.001; ****P < 0.0001

**DRD4 protein expression in clinical colon cancer specimens**

Among 64 paired colon cancer and adjacent non-tumor tissues, 52 tumors (81.3%) and four adjacent tissues (6.3%) were DRD4-positive. Twelve tumors (18.7%) and 60 adjacent tissues (93.7%) were DRD4-negative. Paired analysis showed more frequent DRD4 positivity in tumors (P < 0.001; Supplementary Table S4).

DRD4 immunoreactivity was associated with T stage (P = 0.043) and vascular invasion (P = 0.016; Table 1). It was not significantly associated with sex, age, tumor location, N stage, M stage, or perineural invasion (all P > 0.05).

**Table 1** Association between DRD4 immunoreactivity and clinicopathological characteristics in 64 patients with colon cancer

| Characteristic | Category | DRD4-positive, n (%) | DRD4-negative, n (%) | P-value |
|---|---|---|---|---|
| Sex | Male (n = 34) | 29 (85.3) | 5 (14.7) | 0.378 |
| | Female (n = 30) | 23 (76.7) | 7 (23.3) | |
| Age, years | ≤66 (n = 17) | 13 (76.5) | 4 (23.5) | 0.718 |
| | >66 (n = 47) | 39 (83.0) | 8 (17.0) | |
| Tumor location | Left colon (n = 18) | 15 (83.3) | 3 (16.7) | 1.000 |
| | Right colon (n = 46) | 37 (80.4) | 9 (19.6) | |
| T stage | ≤T2 (n = 24) | 16 (66.7) | 8 (33.3) | **0.043** |
| | >T2 (n = 40) | 36 (90.0) | 4 (10.0) | |
| N stage | N0 (n = 35) | 29 (82.9) | 6 (17.1) | 0.717 |
| | N1/N2 (n = 29) | 23 (79.3) | 6 (20.7) | |
| M stage | M0 (n = 60) | 49 (81.7) | 11 (18.3) | 0.574 |
| | M1 (n = 4) | 3 (75.0) | 1 (25.0) | |
| Vascular invasion | Absent (n = 22) | 14 (63.6) | 8 (36.4) | **0.016** |
| | Present (n = 42) | 38 (90.5) | 4 (9.5) | |
| Perineural invasion | Absent (n = 33) | 25 (75.8) | 8 (24.2) | 0.341 |
| | Present (n = 31) | 27 (87.1) | 4 (12.9) | |

Data are presented as n (%), with percentages calculated within each clinicopathological subgroup. P values were calculated using Fisher's exact test when an expected cell count was <5; otherwise, Pearson's chi-square test was used. Bold values indicate $P < 0.05$.

## Establishment of a DRD4-knockdown cell model

All three DRD4-targeting siRNAs reduced DRD4 mRNA expression in RKO cells at 24 hours. si-DRD4-2 produced the greatest reduction ($P < 0.0001$) and was used in subsequent experiments (Fig. 8a).

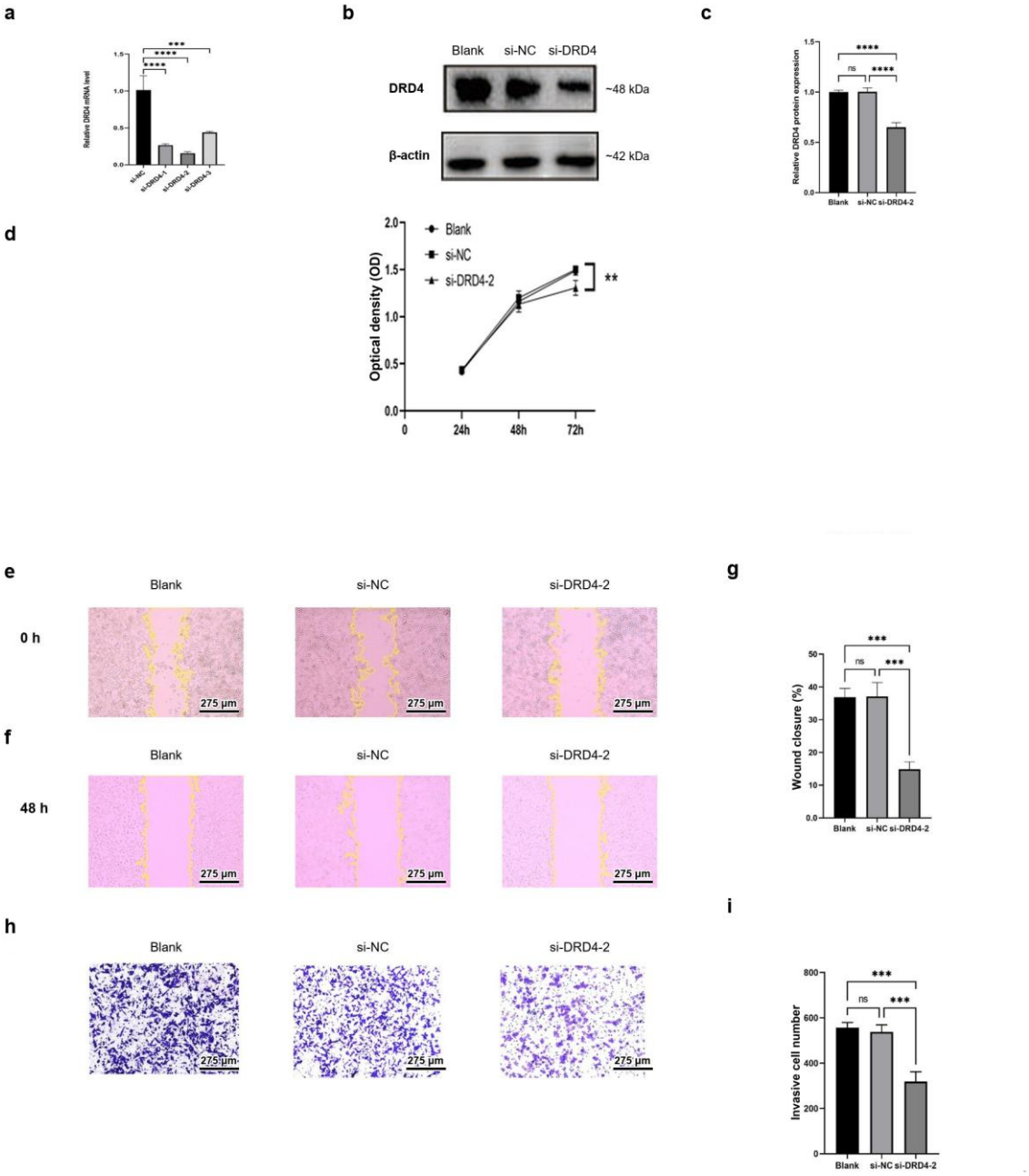
At 48 hours, relative DRD4 protein abundance was lower in si-DRD4-2 cells than in untreated and si-NC controls ($P < 0.0001$; Fig. 8b and c). The two control groups did not differ significantly.

## DRD4 silencing is associated with reduced RKO cell viability, migration and invasion

CCK-8 signals were lower after DRD4 silencing. At 72 hours, optical density (OD) values were 1.485 ± 0.045, 1.501 ± 0.021, and 1.306 ± 0.079 in untreated, si-NC, and si-DRD4-2 cells, respectively. The si-DRD4-2 value was lower than both control values ($P < 0.01$; Fig. 8d).

The 48-hour wound-closure rates were 36.83% ± 2.69%, 37.09% ± 4.04%, and 14.84% ± 2.21% in untreated, si-NC, and si-DRD4-2 cells, respectively. The rate after DRD4 silencing was lower than both control rates ($P < 0.001$; Fig. 8e-g).

In Matrigel-coated Transwell assays, invasive cell counts were 557 ± 23, 538 ± 30, and 318 ± 43 in untreated, si-NC, and si-DRD4-2 cells, respectively. The si-DRD4-2 count was lower than both control counts ($P < 0.001$; Fig. 8h and i). Together, these assays linked DRD4 silencing to reduced RKO cell viability, migration, and invasion.




236

237 Fig. 8 DRD4 silencing and RKO cell phenotypes. (a) DRD4 mRNA knockdown
238 efficiencies of three siRNAs. (b) Representative Western blots of DRD4 (~48 kDa)
239 and β-actin (~42 kDa) in untreated (Blank), negative-control siRNA (si-NC), and si-
240 DRD4 cells (selected si-DRD4-2 construct). (c) Densitometric quantification of DRD4
241 normalized to β-actin. (d) CCK-8 optical density (OD) measurements at 24, 48, and
242 72 h. (e, f) Wound-healing images of the Blank, si-NC, and si-DRD4-2 groups at 0
243 and 48 h, respectively. (g) Wound-closure rate. (h) Matrigel-coated Transwell
244 images. Scale bars in (e), (f), and (h), 275 μm. (i) Quantification of invasive cells.
245 Data are presented as mean ± standard deviation from n = 3 independent
246 experiments. ns, not significant; **P < 0.01; ***P < 0.001; ****P < 0.0001. Full-length,
247 unprocessed blot images are provided in the Supplementary Blot File

## Discussion

The seven-gene risk score stratified disease-free survival in TCGA-COAD and retained 1- and 3-year discrimination in GSE38832, although its 5-year AUC declined to 0.58. The score remained independently associated with disease-free survival after adjustment for age and tumor stage. Paired-tissue and loss-of-function analyses further supported DRD4 as a candidate biomarker, while pathway analyses linked the risk groups to metabolic and immune programs.

External performance was time-dependent, with weaker discrimination at 5 years than at earlier time points. Prediction models require calibration, evaluation across settings, comparison with established clinical models, and structured risk-of-bias assessment. [24,37-39] The current score therefore requires evaluation in additional cohorts before its transportability or incremental prognostic value can be established.

The pathway results connected the risk score to regulated cell death and tumor metabolism. Ferroptosis depends on lipid composition, iron availability, cystine uptake, glutathione metabolism, GPX4, and parallel antioxidant systems such as FSP1-coenzyme Q10. [8,10,11,13-15,40] Mitochondrial tricarboxylic acid-cycle and electron-transport-chain activity can promote ferroptosis during cysteine deprivation. [40] Cysteine depletion induces tumor ferroptosis in vivo, [41] while radiotherapy and immunotherapy can enhance lipid oxidation through SLC7A11 repression. [17] The enrichment of mitochondrial and oxidative phosphorylation programs is consistent with this metabolic context.

Disulfidptosis links cystine transport and NADPH availability to glucose metabolism and actin-cytoskeleton integrity. [10,18,19] SLC7A11-high cells may resist ferroptosis under nutrient-replete conditions but become vulnerable to disulfide stress during glucose limitation. The observed coexpression patterns may therefore reflect a broader metabolic state shared by these cell-death pathways.

The risk groups also differed in immune-cell enrichment scores and immune checkpoint gene expression. The lower enrichment of several potentially antitumor immune-cell populations in the high-risk group may indicate a less favorable immune context. This interpretation is relevant because the density and spatial distribution of tumor-infiltrating lymphocytes are associated with colorectal cancer outcomes. [42-44] However, the TIDE result remains a computational prediction and does not establish treatment response.

DRD4 had the largest positive coefficient in the risk score and was more frequently positive in tumor than in adjacent tissue. DRD4 positivity was also associated with T stage and vascular invasion. Silencing DRD4 reduced RKO cell viability, migration, and invasion. These findings align with evidence that DRD4 can promote colorectal cancer metastasis through transforming growth factor beta receptor and Smad signaling and with studies targeting DRD4 in other tumors. [47,48]

Yi et al. developed a DRD4/SLC2A3 model using cohorts that included GSE38832 and evaluated both markers by immunohistochemistry. [23] Lee et al. also identified DRD4 as an adverse prognostic candidate through machine learning, an independent clinical cohort, and cell-based experiments. [49] The present study extends this evidence by combining a complete seven-gene formula, external evaluation, 64 paired tissues, and DRD4 loss-of-function experiments within one analytical framework.

Other genes in the signature also have established links to colorectal cancer biology. HOTAIR expression has been associated with adverse outcomes, [50,51] and FABP4 can promote fatty acid transport, invasion, and metastasis. [52] MPC1 loss favors glycolytic metabolism and intestinal tumor initiation, [53] while FNDC5/irisin expression has been associated with clinical stage. [54]

Several limitations define the scope of these findings. Development in TCGA-COAD and evaluation in one microarray cohort limit conclusions about transportability and the fixed cutoff. Multistage variable selection and the absence of direct comparisons with clinical-only or published molecular models leave incremental prognostic value uncertain. The immune-cell and TIDE analyses were computational and were not tested in patients receiving immunotherapy. Finally, the DRD4 experiments used tissues from one center and one cell line without rescue, in vivo, or direct ferroptosis and disulfidptosis assays. Additional cohorts and mechanistic experiments should address these specific uncertainties.

The seven-gene risk score stratified disease-free survival in TCGA-COAD and retained short- and intermediate-term discrimination in GSE38832. Risk groups differed in metabolic, mitochondrial, cell-cycle, and immune-related transcriptional programs. DRD4 was more frequently positive in tumor tissue, and its silencing reduced RKO cell viability, migration, and invasion.

These findings support further evaluation of the seven-gene signature and DRD4 as prognostic candidates. Multicenter validation, comparison with established clinical models, and direct mechanistic studies are needed to define their reproducibility and clinical value.

# Methods

### Study design, reporting framework and data sources

This retrospective study combined prognostic model development, external evaluation, and experimental assessment of a candidate gene. Reporting followed the TRIPOD+AI statement. [24] Transcriptomic and clinical data were downloaded for 471 tumors and 41 adjacent non-tumor samples from TCGA-COAD. After excluding cases with missing survival data or survival shorter than 30 days, 424 patients remained for survival analysis. Differential expression analysis included 424 tumors and 41 adjacent non-tumor samples. The external GSE38832 cohort

comprised 122 colon cancer samples with survival data generated on the Affymetrix GPL570 platform. [25]

## Operational definition of candidate genes

We defined candidate genes as FerrDb ferroptosis-related genes coexpressed with disulfidptosis-related genes. After removing duplicates, 564 ferroptosis-related genes were obtained from FerrDb V2.0. [26] The 23 disulfidptosis-related genes defined by Liu et al. were SLC7A11, GYS1, NDUFS1, NDUFA11, NUBPL, NCKAP1, LRPPRC, SLC3A2, RPN1, ACTN4, ACTB, CD2AP, CAPZB, DSTN, FLNA, FLNB, INF2, IQGAP1, MYH10, MYL6, MYH9, PDLIM1, and TLN1. [18] Pearson correlations were calculated across the TCGA expression matrix. Genes with $|r| > 0.50$ and a two-sided $P < 0.05$ were retained.

## Differential expression and functional enrichment analyses

The limma package was used to compare gene expression between colon cancer and adjacent non-tumor tissues. Differentially expressed genes were defined by an absolute $\log_2$ fold change greater than 1 and a Benjamini-Hochberg false discovery rate (FDR) below 0.05. [27] Gene Ontology (GO) enrichment and Kyoto Encyclopedia of Genes and Genomes (KEGG) pathway analyses used KEGG pathway data. [28-30] Analyses were implemented in clusterProfiler, with P values adjusted for multiple comparisons. [31] KEGG pathway annotations and images used in Figs. 1d and 6b are reproduced with permission from Kanehisa Laboratories under the CC BY 4.0 license (permission ref. 262168).

## Development and external evaluation of the prognostic signature

Differentially expressed candidate genes were matched with disease-free survival data in TCGA-COAD. Genes associated with survival in univariable Cox regression ($P < 0.05$) were entered into 10-fold cross-validated LASSO-Cox regression using glmnet. [32] Final variables were selected at $\lambda_{min}$. The risk score equaled the sum of each standardized gene-expression value multiplied by its coefficient. The training-cohort median (-0.09) defined the cutoff applied to both TCGA-COAD and GSE38832.

## Independent prognostic analysis and nomogram

Age, sex, tumor stage, and risk score were evaluated in univariable Cox models. Variables associated with disease-free survival were entered into a multivariable Cox model. Independent prognostic factors were combined in a nomogram for estimating 1-year, 3-year, and 5-year disease-free survival. Time-dependent receiver operating characteristic curves assessed discrimination, and calibration plots assessed agreement between predicted and observed probabilities.

## Pathway and immune microenvironment analyses

Gene set enrichment analysis (GSEA) characterized differences in GO, KEGG, and Reactome pathways between the high- and low-risk groups. Single-sample GSEA estimated enrichment scores for 28 immune-cell populations. [33] We then compared immune-cell scores and immune checkpoint gene expression between risk groups. Tumor Immune Dysfunction and Exclusion (TIDE) scores provided a computational measure of immune evasion. [34]

## Clinical specimens and immunohistochemistry

Tumor and paired adjacent non-tumor tissues were collected from 64 patients with colon cancer. DRD4 expression was assessed by immunohistochemistry. A composite score based on staining intensity and the proportion of positive cells classified samples as positive or negative. Associations were examined for sex, age, tumor location, T/N/M stage, vascular invasion, and perineural invasion. The Ethics Committee of Changshu Hospital Affiliated to Soochow University approved the study (Changshu No. 1 People's Hospital; approval no. 2023 Ethics Review (Application) No. 55). The study complied with the Declaration of Helsinki, and all participants or their authorized representatives provided written informed consent.

## Cell culture, siRNA transfection and expression validation

The RKO cell line was obtained from the Cell Bank of the Chinese Academy of Sciences (Shanghai, China; Catalog No. TCHu116). Human RKO colon cancer cells were cultured at 37 °C in 5% $CO_2$ in medium containing 10% fetal bovine serum and 1% penicillin-streptomycin. Cells were transfected with three independent siRNAs targeting DRD4 or a negative-control siRNA (si-NC). DRD4 mRNA was quantified by reverse-transcription quantitative polymerase chain reaction 24 hours after transfection. Relative expression was calculated using the $2^{-\Delta\Delta Ct}$ method. [35] DRD4 protein was assessed by Western blotting 48 hours after transfection, with β-actin as the loading control. The most efficient siRNA, si-DRD4-2, was used in subsequent experiments. Quantitative PCR experiments followed the MIQE recommendations. [36] Supplementary Tables S1 and S2 list the siRNA and primer sequences, respectively.

## Cell viability, migration and invasion assays

Cell viability after DRD4 silencing was measured with the Cell Counting Kit-8 assay at 24, 48, and 72 hours. For wound-healing assays, the same fields were imaged at 0 and 48 hours, and wound closure was quantified. Transwell inserts were precoated with Matrigel. After 48 hours, invading cells were fixed, stained, and counted. All cell-based experiments were performed in three independent experiments.

### Statistical analysis

Bioinformatic analyses were performed in R. Clinical and cell-based data were analyzed with SPSS version 26.0 and GraphPad Prism version 9.5.0. Continuous variables are reported as mean ± standard deviation. Tests for independent two-group, three-group, and repeated-measures comparisons were selected according to the data distribution and study design. Categorical variables were analyzed with the chi-square test or Fisher's exact test. Paired binary immunohistochemical results were compared with the McNemar test. All tests were two-sided, and $P < 0.05$ indicated statistical significance.

## Acknowledgements

The authors thank The Cancer Genome Atlas and Gene Expression Omnibus projects and their data contributors. Permission to use the KEGG pathway annotations and images was granted by Kanehisa Laboratories (Ref. 262168).

## Author contributions

T.Z. and Y.L. contributed equally to this work. T.Z. contributed to the study design, methodology, bioinformatic and statistical analyses, data interpretation, visualization, and preparation of the original manuscript. Y.L. contributed to the methodology, experimental investigation, validation, data curation, visualization, and preparation of the original manuscript. K.L. contributed to clinical data and specimen collection, investigation, and data curation. Q.C. contributed to immunohistochemical experiments, validation, and interpretation of the experimental results. S.W. contributed to cell-based experiments, data acquisition, and formal analysis. Y.X. contributed to data verification, visualization, and interpretation of the results. J.Z. contributed to the conception and methodology of the study, supervision, project administration, interpretation of the results, and critical revision of the manuscript. J.S. contributed to the conception of the study, funding acquisition, provision of resources, supervision, project administration, and critical revision of the manuscript. All authors reviewed and approved the final manuscript and agreed to be accountable for the work.

## Funding

This work was supported by the Suzhou Science and Technology Development Plan Program (Grant No. SYW2024047) and the Changshu Science and Technology Development Plan Program (Grant No. KCH202501).

## Data availability

TCGA-COAD data are publicly available through the NCI Genomic Data Commons (https://portal.gdc.cancer.gov/projects/TCGA-COAD), and GSE38832 is publicly available through the NCBI Gene Expression Omnibus (https://www.ncbi.nlm.nih.gov/geo/query/acc.cgi?acc=GSE38832). Subject to ethical and institutional restrictions, analysis scripts and additional deidentified experimental data are available from the corresponding author upon reasonable request.

## Ethics approval and consent to participate

The Ethics Committee of Changshu Hospital Affiliated to Soochow University approved the study (Changshu No. 1 People's Hospital; approval no. 2023 Ethics Review (Application) No. 55). The study was conducted in accordance with the Declaration of Helsinki, and all participants or their authorized representatives provided written informed consent.

## Consent for publication

Not applicable.

## Competing interests

The authors declare no competing interests.

## Supplementary Information

Supplementary Information accompanies this manuscript and includes Supplementary Tables S1-S4. Full-length, unprocessed blot images are provided in the Supplementary Blot File.

## References

[1] Bray, F. et al. Global cancer statistics 2022: GLOBOCAN estimates of incidence and mortality worldwide for 36 cancers in 185 countries. CA Cancer J. Clin. 74, 229–263 (2024). https://doi.org/10.3322/caac.21834

[2] Dienstmann, R. et al. Consensus Molecular Subtypes and the Evolution of Precision Medicine in Colorectal Cancer. Nat. Rev. Cancer. 17, 79–92 (2017). https://doi.org/10.1038/nrc.2016.126

[3] Dekker, E., Tanis, P. J., Vleugels, J. L. A., Kasi, P. M. & Wallace, M. B. Colorectal Cancer. Lancet. 394, 1467–1480 (2019). https://doi.org/10.1016/S0140-6736(19)32319-0

[4] Biller, L. H. & Schrag, D. Diagnosis and Treatment of Metastatic Colorectal Cancer: A Review. JAMA. 325, 669–685 (2021). https://doi.org/10.1001/jama.2021.0106

[5] Cancer Genome Atlas Network. Comprehensive molecular characterization of human colon and rectal cancer. Nature. 487, 330–337 (2012). https://doi.org/10.1038/nature11252

[6] Guinney, J. et al. The consensus molecular subtypes of colorectal cancer. Nat. Med. 21, 1350–1356 (2015). https://doi.org/10.1038/nm.3967

[7] Dixon, S. J. et al. Ferroptosis: An iron-dependent form of nonapoptotic cell death. Cell. 149, 1060–1072 (2012). https://doi.org/10.1016/j.cell.2012.03.042

[8] Stockwell, B. R. et al. Ferroptosis: A Regulated Cell Death Nexus Linking Metabolism, Redox Biology, and Disease. Cell. 171, 273–285 (2017). https://doi.org/10.1016/j.cell.2017.09.021

[9] Jiang, X., Stockwell, B. R. & Conrad, M. Ferroptosis: Mechanisms, biology and role in disease. Nat. Rev. Mol. Cell Biol. 22, 266–282 (2021). https://doi.org/10.1038/s41580-020-00324-8

[10] Koppula, P., Zhuang, L. & Gan, B. Cystine Transporter SLC7A11/xCT in Cancer: Ferroptosis, Nutrient Dependency, and Cancer Therapy. Protein Cell. 12, 599–620 (2021). https://doi.org/10.1007/s13238-020-00789-5

[11] Yang, W. S. et al. Regulation of Ferroptotic Cancer Cell Death by GPX4. Cell. 156, 317–331 (2014). https://doi.org/10.1016/j.cell.2013.12.010

[12] Viswanathan, V. S. et al. Dependency of a therapy-resistant state of cancer cells on a lipid peroxidase pathway. Nature. 547, 453–457 (2017). https://doi.org/10.1038/nature23007

[13] Hangauer, M. J. et al. Drug-Tolerant Persister Cancer Cells Are Vulnerable to GPX4 Inhibition. Nature. 551, 247–250 (2017). https://doi.org/10.1038/nature24297

[14] Bersuker, K. et al. The CoQ Oxidoreductase FSP1 Acts Parallel to GPX4 to Inhibit Ferroptosis. Nature. 575, 688–692 (2019). https://doi.org/10.1038/s41586-019-1705-2

[15] Doll, S. et al. FSP1 Is a Glutathione-Independent Ferroptosis Suppressor. Nature. 575, 693–698 (2019). https://doi.org/10.1038/s41586-019-1707-0

[16] Wang, W. et al. $CD8^+$ T cells regulate tumour ferroptosis during cancer immunotherapy. Nature. 569, 270–274 (2019). https://doi.org/10.1038/s41586-019-1170-y

[17] Lang, X. et al. Radiotherapy and Immunotherapy Promote Tumoral Lipid Oxidation and Ferroptosis via Synergistic Repression of SLC7A11. Cancer Discov. 9, 1673–1685 (2019). https://doi.org/10.1158/2159-8290.CD-19-0338

[18] Liu, X. et al. Actin cytoskeleton vulnerability to disulfide stress mediates disulfidptosis. Nat. Cell Biol. 25, 404–414 (2023). https://doi.org/10.1038/s41556-023-01091-2

[19] Liu, X. et al. Cystine transporter regulation of pentose phosphate pathway dependency and disulfide stress exposes a targetable metabolic vulnerability in cancer. Nat. Cell Biol. 22, 476–486 (2020). https://doi.org/10.1038/s41556-020-0496-x

[20] Nie, J. et al. A novel ferroptosis-related gene signature for prognosis prediction in patients with colon cancer. Front. Oncol. 11, 654076 (2021). https://doi.org/10.3389/fonc.2021.654076

[21] Wang, Y., Xia, H. B., Chen, Z. M., Meng, L. & Xu, A. M. Identification of a ferroptosis-related gene signature predictive model in colon cancer. World J. Surg. Oncol. 19, 135 (2021). https://doi.org/10.1186/s12957-021-02244-z

[22] Li, Z. et al. Establishment and validation of a ferroptosis-related signature predicting prognosis and immunotherapy effect in colon cancer. Front. Oncol. 13, 1201616 (2023). https://doi.org/10.3389/fonc.2023.1201616

[23] Yi, N. et al. Development and validation of a prognostic model based on disulfidptosis-related ferroptosis genes: DRD4 and SLC2A3 as biomarkers for predicting prognosis in colon cancer. Transl. Cancer Res. 14, 159–178 (2025). https://doi.org/10.21037/tcr-24-1177

[24] Collins, G. S. et al. TRIPOD+AI statement: updated guidance for reporting clinical prediction models that use regression or machine learning methods. BMJ. 385, e078378 (2024). https://doi.org/10.1136/bmj-2023-078378

[25] Tripathi, M. K. et al. Nuclear factor of activated T-cell activity is associated with metastatic capacity in colon cancer. Cancer Res. 74, 6947–6957 (2014). https://doi.org/10.1158/0008-5472.CAN-14-1592

[26] Zhou, N. et al. FerrDb V2: Update of the manually curated database of ferroptosis regulators and ferroptosis-disease associations. Nucleic Acids Res. 51, D571–D582 (2023). https://doi.org/10.1093/nar/gkac935

[27] Ritchie, M. E. et al. limma powers differential expression analyses for RNA-sequencing and microarray studies. Nucleic Acids Res. 43, e47 (2015). https://doi.org/10.1093/nar/gkv007

[28] Kanehisa, M., Furumichi, M., Sato, Y., Matsuura, Y. & Ishiguro-Watanabe, M. KEGG: biological systems database as a model of the real world. Nucleic Acids Res. 53, D672–D677 (2025). https://doi.org/10.1093/nar/gkae909

[29] Kanehisa, M. Toward understanding the origin and evolution of cellular organisms. Protein Sci. 28, 1947–1951 (2019). https://doi.org/10.1002/pro.3715

[30] Kanehisa, M. & Goto, S. KEGG: Kyoto Encyclopedia of Genes and Genomes. Nucleic Acids Res. 28, 27–30 (2000). https://doi.org/10.1093/nar/28.1.27

[31] Wu, T. et al. clusterProfiler 4.0: A universal enrichment tool for interpreting omics data. Innovation. 2, 100141 (2021). https://doi.org/10.1016/j.xinn.2021.100141

[32] Friedman, J., Hastie, T. & Tibshirani, R. Regularization paths for generalized linear models via coordinate descent. J. Stat. Softw. 33, 1–22 (2010). https://doi.org/10.18637/jss.v033.i01

[33] Hänzelmann, S., Castelo, R. & Guinney, J. GSVA: Gene set variation analysis for microarray and RNA-seq data. BMC Bioinformatics. 14, 7 (2013). https://doi.org/10.1186/1471-2105-14-7

[34] Jiang, P. et al. Signatures of T cell dysfunction and exclusion predict cancer immunotherapy response. Nat. Med. 24, 1550–1558 (2018). https://doi.org/10.1038/s41591-018-0136-1

[35] Livak, K. J. & Schmittgen, T. D. Analysis of relative gene expression data using real-time quantitative PCR and the $2^{-\Delta\Delta Ct}$ method. Methods. 25, 402–408 (2001). https://doi.org/10.1006/meth.2001.1262

[36] Bustin, S. A. et al. The MIQE Guidelines: Minimum Information for Publication of Quantitative Real-Time PCR Experiments. Clin. Chem. 55, 611–622 (2009). https://doi.org/10.1373/clinchem.2008.112797

[37] Steyerberg, E. W. et al. Assessing the Performance of Prediction Models: A Framework for Traditional and Novel Measures. Epidemiology. 21, 128–138 (2010). https://doi.org/10.1097/EDE.0b013e3181c30fb2

[38] McShane, L. M. et al. REporting Recommendations for Tumour MARKer Prognostic Studies (REMARK). Br. J. Cancer. 93, 387–391 (2005). https://doi.org/10.1038/sj.bjc.6602678

[39] Wolff, R. F. et al. PROBAST: a tool to assess the risk of bias and applicability of prediction model studies. Ann. Intern. Med. 170, 51–58 (2019). https://doi.org/10.7326/M18-1376

[40] Gao, M. et al. Role of Mitochondria in Ferroptosis. Mol. Cell. 73, 354–363.e3 (2019). https://doi.org/10.1016/j.molcel.2018.10.042

[41] Badgley, M. A. et al. Cysteine Depletion Induces Pancreatic Tumor Ferroptosis in Mice. Science. 368, 85–89 (2020). https://doi.org/10.1126/science.aaw9872

[42] Pagès, F. et al. International validation of the consensus Immunoscore for the classification of colon cancer: A prognostic and accuracy study. Lancet. 391, 2128–2139 (2018). https://doi.org/10.1016/S0140-6736(18)30789-X

[43] Galon, J. et al. Type, Density, and Location of Immune Cells within Human Colorectal Tumors Predict Clinical Outcome. Science. 313, 1960–1964 (2006). https://doi.org/10.1126/science.1129139

[44] Mlecnik, B. et al. Integrative Analyses of Colorectal Cancer Show Immunoscore Is a Stronger Predictor of Patient Survival Than Microsatellite Instability. Immunity. 44, 698–711 (2016). https://doi.org/10.1016/j.immuni.2016.02.025

[45] André, T. et al. Pembrolizumab in Microsatellite-Instability-High Advanced Colorectal Cancer. N. Engl. J. Med. 383, 2207–2218 (2020). https://doi.org/10.1056/NEJMoa2017699

[46] Overman, M. J. et al. Durable Clinical Benefit with Nivolumab Plus Ipilimumab in DNA Mismatch Repair-Deficient/Microsatellite Instability-High Metastatic Colorectal Cancer. J. Clin. Oncol. 36, 773–779 (2018). https://doi.org/10.1200/JCO.2017.76.9901

[47] Zhou, Y., Tang, J., Weng, M., Zhang, H. & Lai, M. DRD4 interacts with TGF-β receptors to drive colorectal cancer metastasis independently of dopamine signaling pathway. Adv. Sci. (Weinh.). 12, 2413953 (2025). https://doi.org/10.1002/advs.202413953

[48] Dolma, S. et al. Inhibition of dopamine receptor D4 impedes autophagic flux, proliferation, and survival of glioblastoma stem cells. Cancer Cell. 29, 859–873 (2016). https://doi.org/10.1016/j.ccell.2016.05.002

[49] Lee, C. J. et al. Machine learning with in silico analysis markedly improves survival prediction modeling in colon cancer patients. Cancer Med. 12, 7603–7615 (2023). https://doi.org/10.1002/cam4.5420

[50] Huang, K. B. et al. HOTAIR mediates tumorigenesis through recruiting EZH2 in colorectal cancer. J. Cell. Biochem. 120, 6071–6077 (2019). https://doi.org/10.1002/jcb.27893

[51] Svoboda, M. et al. HOTAIR long non-coding RNA is a negative prognostic factor not only in primary tumors, but also in the blood of colorectal cancer patients. Carcinogenesis. 35, 1510–1515 (2014). https://doi.org/10.1093/carcin/bgu055

[52] Tian, W. et al. FABP4 promotes invasion and metastasis of colon cancer by regulating fatty acid transport. Cancer Cell Int. 20, 512 (2020). https://doi.org/10.1186/s12935-020-01582-4

[53] Bensard, C. L. et al. Regulation of Tumor Initiation by the Mitochondrial Pyruvate Carrier. Cell Metab. 31, 284–300.e7 (2020). https://doi.org/10.1016/j.cmet.2019.11.002

[54] Wozniak, S., Nowinska, K., Chabowski, M. & Dziegiel, P. Significance of Irisin (FNDC5) Expression in Colorectal Cancer. In Vivo. 36, 180–188 (2022). https://doi.org/10.21873/invivo.12689

## Supplementary Files

This is a list of supplementary files associated with this preprint. Click to download.

- wb.pdf
- SupplementaryInformation.docx